Manuscript prepared for Ocean Sci.
with version 2015/04/24 7.83 Copernicus papers of the LaTeX class copernicus.cls.
Date: 6 February 2017

A harmonic projection and least–squares method for quantifying *equatorial* wave activity

Andrew Delman[1], Janet Sprintall[1], Julie McClean[1], and Lynne Talley[1]

[1]Scripps Institution of Oceanography, University of California–San Diego, La Jolla, California, USA.

Correspondence to: Corresponding author: Andrew S. Delman, now at the Jet Propulsion Laboratory, Pasadena, California, USA. (Andrew.S.Delman@jpl.nasa.gov)

Abstract. A new method for isolating *the sea surface height signals associated with equatorial Kelvin and Rossby waves is* presented and applied to *altimetric* sea level anomaly (SLA) observations in the tropical Indian *and Pacific* oceans. The method *projects wave functions representing propagating equatorial wave modes* onto the SLA data*. Each wave function is three-dimensional: the product of a meridional profile for a given wave mode derived from shallow-water theory, and a harmonic function that propagates zonally within a phase speed range close to that of the wave mode. Moreover, the wave functions are tapered within the zonal domain, to approximate the forcing and dissipation of waves within the domain, and to minimize aliasing of waves that only propagate across part of the ocean basin.* After projections in all three dimensions have been carried out, least-squares methods are applied to *recover* the non-orthogonal wave function coefficients and minimize the misfit of their along-waveguide forcing and dissipation. *The result of these calculations are mode-associated SLA fields associated with Kelvin waves and with the first 5 meridional Rossby wave modes, which can be used as a proxy for the waves' amplitude.*

The mode SLA field results are validated by correlation with the original SLA data over a 23-year period, as well as by correlation with the residual SLA field from removing the mode SLA. The spatial distribution of the 1st meridional mode Rossby wave correlations also confirms our choices for the value of c, the (1st baroclinic) Kelvin wave phase speed. Compared to earlier methods that used only the meridional structure to decompose equatorial wave modes, the mode SLA clarifies the signals from freely-propagating intraseasonal waves, such as those that are forced by MJO-related winds. As this method of decomposition favors propagating waves but does not constrain their phase speed to a specific value, the mode SLA may provide the opportunity to study weakly nonlinear aspects of these waves by comparison with linear models.

1 Introduction

The quantification of ocean variability associated with equatorial long waves is a topic of great importance for understanding the tropical ocean and its role in climate. Since the advent of satellite

altimetry, the surface manifestations of these waves and the wind forcing driving them have been tracked in datasets that now comprise over 20 years of continuous global coverage (e.g., Delcroix et al., 1994; Susanto et al., 1998; Boulanger and Menkes, 1999; Drushka et al., 2010). However, to use these observations to better understand the behavior of these planetary waves and their relationship to climate variability, analysis techniques are needed that target the specific signatures of Kelvin and Rossby waves in satellite observations.

A variety of techniques have been employed to quantify equatorial long wave activity from satellite observations; these range from the application of sophisticated data assimilation techniques to meridional projections of sea level anomaly (SLA) data. The data assimilation approaches generally use a linear wave-propagation model, along with Kalman filters (e.g., Miller and Cane, 1989; Fu et al., 1993) or adjoints (e.g., Thacker and Long, 1988; Long and Thacker, 1989a, b) to incorporate observations. These techniques are particularly useful for cases where observations are sparse and error–prone, as is often the case for in-situ measurements, and also during the earlier years of satellite observations when spatial resolution was low (e.g., Geosat). As the spatial and temporal coverage of altimeter-derived remote sensing data increased, it was conceivable to estimate Kelvin and Rossby wave activity using solely meridional projections of SLA data, or a combination of SLA and current observations. Cane and Sarachik (1981) showed that vectors containing SLA and surface current profiles associated with a given vertical Kelvin wave mode and its associated meridional Rossby wave modes are orthogonal; this orthogonality provided the basis for an equatorial wave decomposition in numerous studies (e.g., Delcroix et al., 1994; Yuan et al., 2004; Yuan and Liu, 2009). Boulanger and Menkes (1995, 1999), BM9599 hereafter, also carried out a decomposition using only meridional projections of SLA data that were reasonably consistent with projections derived from in-situ moorings. However, the decomposition of Kelvin and Rossby wave modes based on meridional projections of SLA alone are not orthogonal, and as Yuan et al. (2004) notes, this necessitates the inversion of an ill-conditioned matrix. An alternative approach used complex EOFs of SLA to separate Rossby and Kelvin wave signals in the equatorial Pacific (Susanto et al., 1998); one limitation of this method is that complex EOFs by definition constrain the along-waveguide and across-waveguide length scales of the waves, while shallow-water theory only constrains the across-waveguide length scale.

Here we *outline a method that projects three-dimensional propagating wave functions on SLA values, to estimate the components of equatorial wave modes in the SLA field. In contrast with the work of BM9599 which projected one-dimensional meridional profiles onto SLA, our projection method simultaneously uses the meridional profile and the phase speed of each wave mode to isolate its SLA signal. The method requires only the SLA data as input, and the resulting mode SLA highlights intraseasonal propagating features.* The paper is structured as follows: Section 2 describes the data and the harmonic projection and least-squares method *used to obtain the mode SLA field*. Section 3 *assesses the spatial distribution of the relationship between the mode SLA computed and the original*

SLA field, examining where inaccuracies in the estimation of mode amplitudes may exist. Section 4 illustrates characteristics of the mode SLA fields in the two ocean basins, and compares the amplitudes to those obtained by Boulanger and Menkes (1999). Section 5 summarizes the strengths and weaknesses of the method, and considers *possible applications and adjustments to the method in future studies*.

2 Method

2.1 Data

*I*n this study, our methodology *is applied to* AVISO Ssalto/Duacs *gridded maps of absolute dynamic topography (MADT), which are available at 1/4° spatial resolution and daily temporal resolution from the Centre National d'Études Spatiales (Ducet et al., 2000). The analysis discussed here uses the delayed-time, merged product which is produced from all the available altimetry data starting in 1993; we make use of the data from January 1993 to December 2015. The resolution of this dataset is more than sufficient to track the equatorial long waves targeted in this study, whose maxima/minima generally have meridional scales >1°, zonal scales >5°, and monthly or longer temporal scales (e.g., Boulanger and Menkes, 1999; Nagura and McPhaden, 2012). However, we note that the projections as described in Section 2.2 could be applied to a non-gridded (e.g., alongtrack) dataset as well, provided the data have sufficient spatiotemporal resolution and coverage.*

Before the projections are applied, the absolute dynamic topography data have their meridional mean and trend between 15°S and 15°N removed at each longitude and time, to obtain the detrended SLA data values η_d; this excludes signals from large-scale meridional pressure gradients that are unrelated to equatorial wave activity. The SLA data are then band-passed to create a low-passed and a high-passed SLA field; the projections and least-squares deconvolution are applied to the low-passed and high-passed fields separately. The lower-frequency wave functions are projected onto the full 23-year low-passed SLA field before the least-squares deconvolution is carried out, while the higher-frequency intraseasonal wave functions are projected onto the high-passed SLA field and deconvolved in overlapping 2-year segments (1993–1994, 1994–1995, 1995–1996, etc.). At the end of the analysis, the low- and high-passed mode SLA components are summed together, with the results from the high-frequency 2-year segments combined by tapering the overlapping segments together.

2.2 *SLA* projections

The distinctive feature of this equatorial wave analysis compared to previous decompositions (e.g., Delcroix et al., 1994, BM9599) is the use of three-dimensional harmonic "wave" functions to be projected onto the detrended SLA. Each wave function $F^q_{m,n,\varsigma,s}$ is the product of three components

$$F^q_{m,n,\varsigma,s}(x,y,t) = \phi_q(y) G_{m,n,\varsigma}(x,t) H_s(x) \tag{1}$$

namely, the meridional structure function $\phi_q(y)$ for meridional mode q, zonally-propagating harmonic functions $G_{m,n,\varsigma}(x,t)$, and a taper function $H_s(x)$. The parameters m, n, and ς indicate respectively the wavenumber, frequency, and phase of the function, while s indicates the tapering location of the function as will be discussed in Section 2.2.3. (The coordinates x, y, and t are the zonal, meridional, and time coordinates respectively.) Each wave function is projected onto the SLA data between latitudes 15°S and 15°N, to resolve the meridional structures of equatorial Kelvin waves and the first 5 meridional Rossby wave modes.

2.2.1 Meridional structure function

The meridional structure functions are derived from the eigenfunction solutions of the shallow-water momentum and mass conservation equations, with the Coriolis parameter f varying as a function of y (e.g., Matsuno, 1966; Moore, 1968; Gill and Clarke, 1974). The form that these solutions take for pressure perturbations (and therefore for SLA) is

$$\phi_{-1}(y) = \frac{1}{\sqrt{2}} \psi_0 \tag{2}$$

$$\phi_q(y) = \sqrt{\frac{q(q+1)}{2(2q+1)}} \left(\frac{\psi_{q+1}}{\sqrt{q+1}} + \frac{\psi_{q-1}}{\sqrt{q}} \right) \quad \text{for} \, q > 0 \tag{3}$$

after Boulanger and Menkes (1995), with ψ_q a solution (bounded as $y \to \pm\infty$) to the eigenvalue problem posed by the shallow-water equation for meridional velocity v

$$\frac{\partial^2 v}{\partial {y_*}^2} + (2q + 1 - y_*^2) v = 0 \tag{4}$$

with $\beta = \partial f / \partial y$ and non-dimensional $y_* = (\beta/c)^{1/2} y$. (The trivial solution $v = 0$ for (4) corresponds to $q = -1$, the Kelvin wave mode.) The value of the equatorial Kelvin wave phase speed c was taken to be 2.5 m s^{-1} in the Indian Ocean, based on earlier observational estimates for the first baroclinic wave phase speed (e.g., Nagura and McPhaden, 2012). In the Pacific Ocean, c is taken to be 2.5 m s^{-1} in the western part of the basin (e.g., Kessler and McPhaden, 1995; Hendon

et al., 1998), but east of 180° longitude this value is gradually decreased to 2.0 m s^{-1} at the eastern boundary due to the decrease in phase speed from the shoaling of the thermocline (e.g., Giese and Harrison, 1990). More details on the derivation of these structure functions are available from other sources (e.g., Matsuno, 1966; Boulanger and Menkes, 1995, , Sec. A1). The analytical form of ψ_q for constant β values can also be expressed in terms of Hermite polynomials (e.g., Matsuno, 1966); in our case ψ_q were solved for numerically, with β values allowed to vary slightly as a function of latitude.

2.2.2 Zonally-propagating harmonic functions

The zonally-propagating harmonic functions $G_{m,n,\varsigma}(x,t)$ take the form

$$G_{m,n,1}(x,t) = \cos\left[2\pi\left(k_m x - f_n t\right)\right] \tag{5}$$

$$G_{m,n,2}(x,t) = \sin\left[2\pi\left(k_m x - f_n t\right)\right] \tag{6}$$

with $\varsigma = 1$ indicating a cosine function (i.e. phase = 0°), and $\varsigma = 2$ indicating a sine function (i.e. phase = 90°). Values of k_m can vary in the range $k_m = 0, \pm 1/(x_L + \Delta x), \pm 2/(x_L + \Delta x)$, ... for $|k_m| \leq 1/\Delta x$, with x_L equal to the span of the ocean basin at the equator, and $\Delta x = 5°$. (Δx is chosen to be much larger than the actual zonal resolution of the data, as the long waves of interest in this study generally have large zonal scales.) The wave functions are projected on to the low- and high-passed SLA data separately as described in Section 2.1. For projections onto the low-passed SLA data, values of f_n can vary in the range $f_n = 0, 1/t_L, 2/t_L$, ... for $f_n \leq 1/\Delta t$, with t_L = 23 years (the time span of the entire dataset) and Δt = 2/9 years ≈ 81 days (sufficient to resolve periods longer than 162 days, or semiannual and lower frequencies). For the high-passed data, which are projected in 2-year segments, t_L = 2 years and f_n varies at intervals of $1/t_L$ in the frequency range corresponding to periods of approximately 20–150 days (the intraseasonal frequency band), with Δt = 10 days. As with Δx, Δt can be longer than the actual time resolution of the data.

2.2.3 Taper functions

Lastly, the taper functions $H_s(x)$ are included to improve the representation of waves that are forced and dissipate within the ocean basin. This is particularly important for equatorial long waves whose zonal wavelength may be as long or longer than the width of the ocean basin. When propagating waves change amplitude, a portion of the wave activity is aliased into adjacent wavenumbers and frequencies; this presents a potential issue for correctly identifying the mode of low-wavenumber equatorial long waves. The tapers help ensure that a low-wavenumber, eastward-propagating Kelvin

wave generated in the middle of the basin is identified as such. The taper functions (Figure 1) take the form

$$H_s(x) = \begin{cases} 0, & x \le x_s - \Delta x \\ \left(1 - \frac{x_s - x}{\Delta x}\right), & x_s - \Delta x < x < x_s \\ 1, & x \ge x_s \end{cases} \quad (7)$$

The tapering location x_s is varied within the range $x_s = 0, \Delta x, 2\Delta x, ...$ for $x_s \le x_L$. (The analysis is carried out with two different x-coordinates: $x = 0$ at the western boundary and x increases eastward, and $x = 0$ at eastern boundary and x increases westward. The mode SLA obtained using the two coordinate systems are averaged at the end of the analysis; this approach is used to minimize any bias that would be introduced at either the western or eastern boundary due to the technique.)

2.2.4 Projecting wave functions for each mode

The wave functions $F^q_{m,n,\varsigma,s}$ for the Kelvin wave mode $q = 0$ and the first five meridional Rossby wave modes $q = 1, ..., 5$ are projected onto the detrended SLA. The wave functions for each mode q consist of the corresponding meridional structure function ϕ_q, a full range of possible taper functions H_s as described in Section 2.2.3, and the propagating harmonic functions $G_{m,n,\varsigma}$ that have phase speeds f_n/k_m within the ranges given in Table 1. (Note: in the Pacific, where the input phase speed c varies across the basin, c_{min} is computed using c = 2.0 m s^{-1}, and c_{max} is computed using c = 2.5 m s^{-1}. Hence the ranges specified in Table 1 will have some overlap, but the associated wave functions are still distinct because of their meridional structures.)

As part of the signal for fast-propagating waves is aliased into the zero wavenumber band, $G_{m,n,\varsigma}$ functions for which $k_m = 0$ are also projected for frequency values $f_n < \Delta k |c_{\max}|$, with $\Delta k = 1/(x_L + \Delta x)$ the lowest-magnitude non-zero wavenumber resolved in this analysis, and $c_{\max}$ the maximum (magnitude) phase speed for that mode as given in Table 1.

Prior to projecting, each wave function $F^q_{m,n,\varsigma,s}$ has the meridional mean and trend removed in the same way that the SLA data are processed. Then the projection of each wave function onto the SLA data is carried out, point-by-point in the x, y, t domain. If $\mathbf{d}$ is a vector consisting of all of the x, y, t meridionally-detrended SLA data point values η_d, and $\mathbf{F}$ is a matrix with each column consisting of the x, y, t values of a wave function $F^q_{m,n,\varsigma,s}$, then the projection value for column α of $\mathbf{F}$ (i.e., $\mathbf{F}_\alpha$) is given by

$$p_\alpha = \left[(\mathbf{F}_\alpha)^T \mathbf{F}_\alpha \right]^{-2} (\mathbf{F}_\alpha)^T \mathbf{d} \quad (8)$$

with the first part of the right-hand side (containing the exponent -2) normalizing the projection. The resulting scalars p_α are the elements of a vector $\mathbf{p}$ containing the projection values. Alternatively (8) can be expressed in terms of a projection operator $\mathbf{P}$

$$\mathbf{p} = \mathbf{P}\mathbf{d} \tag{9}$$

We note that if all of the wave functions (i.e., the columns of $\mathbf{F}$) were independent, then (8) would be equivalent to a linear regression of each wave function onto the SLA data, yielding coefficients that could be used to compute the SLA associated with each mode. However, the wave functions are not independent; furthermore, a linear regression applied directly to the SLA data weights the misfit to points far from the equator (where wave amplitudes are negligible) just as heavily as points near the equator where these waves constitute a large fraction of the SLA variance. Instead of regressing the SLA data directly, a cost function of the misfit to projection values in $\mathbf{p}$ is minimized to find optimal coefficients for the wave functions, as described in Section 2.3.

2.3 Least-squares deconvolution of wave function coefficients

Given the projection values based on the SLA data, the next objective is to find a set of "true" wave function coefficients $\mathbf{m}$ that can most accurately account for the observation-based projection values in $\mathbf{p}$, within desired parameters. To achieve this, we seek to solve the system $\mathbf{Fm} = \mathbf{d}$ for the coefficients $\mathbf{m}$, such that the following cost function is minimized

$$L = [\mathbf{DP}(\mathbf{Fm}) - \mathbf{Dp}]^T [\mathbf{DP}(\mathbf{Fm}) - \mathbf{Dp}] + [w(\mathbf{P}(\mathbf{Fm}) - \mathbf{p})]^T [w(\mathbf{P}(\mathbf{Fm}) - \mathbf{p})] + \left[(\mathbf{\Lambda m})^T \mathbf{m}\right] \tag{10}$$

There are three parts to this cost function. The first part minimizes the misfit to the change in the projection values along the waveguide $\mathbf{Dp}$, the second part minimizes the misfit to the projection values $\mathbf{p}$, and the third part establishes a preference for values of $\mathbf{m}$ that are not too large. The matrix $\mathbf{D}$ is the finite difference operator for $s > 1$ projections, and the identity operator for $s = 1$ projections (i.e., the finite difference between zero and the $s = 1$ projection value). *The scalar value w and the diagonal matrix $\mathbf{\Lambda}$ are both adjustable parameters that set the relative weighting of the parts of the cost function. A number of possible combinations of these parameters were tested to determine which values generated the solution that explains the most SLA variance. The optimal value chosen for w is 0.2; the diagonal of $\mathbf{\Lambda}$ has values of 2 for entries corresponding to $s = 1$ wave functions (i.e., the functions that span the entire ocean basin). For the $s > 1$ wave functions, values of 20 are used in the Indian Ocean, and 5 in the Pacific Ocean. The different values in the two basins are likely needed to suppress high-wavenumber variability in the Indian Ocean that is*

not well described by the low-wavenumber limits of the equatorial wave dispersion relation (e.g. Matsuno, 1966).

The formula for the coefficients $\mathbf{m}$ *that minimizes the cost function (10) is*

$$\mathbf{m} = \left[(\mathbf{DPF})^T \mathbf{DFP} + (w\mathbf{PF})^T w\mathbf{PF} + \mathbf{\Lambda}\right]^{-1} \left[(\mathbf{DPF})^T \mathbf{Dp} + (w\mathbf{PF})^T w\mathbf{p}\right] \tag{11}$$

Once the coefficients $\mathbf{m}$ *are obtained, then the contribution to SLA from wave functions associated with each mode* q *can be summed up to yield the contribution to SLA from that mode* η_q *(the mode SLA):*

$$\eta_q(x,y,t) = \sum_q \mathbf{m}^q_{m,n,c,s} F^q_{m,n,\varsigma,s}(x,y,t) \tag{12}$$

with $\mathbf{m}^q_{m,n,c,s}$ *the (scalar) coefficient from* $\mathbf{m}$ *that corresponds to the wave function* $F^q_{m,n,\varsigma,s}$*. (Note: the meridional structure functions within* $F^q_{m,n,\varsigma,s}$ *have their original meridional means and trends added back to them before the mode SLA is calculated.)*

3 Validation and characteristics of the mode SLA

To assess how accurately the mode SLA represents the true contribution of each meridional mode to the SLA field, two correlation metrics are computed. The first correlates the temporal variation of SLA associated with each mode to that of the original, meridionally-detrended SLA $r(\eta_q, \eta_d)$*. Robust values of this correlation at latitudes where the given wave mode* q *is known to make a leading-order contribution to SLA variability confirm that the sign and meridional structure of the wave mode is well represented. The other metric is the correlation of the temporal variation of mode SLA to the residual SLA* η_r*, which is* η_d *with the sum of the mode SLA from all of the projected modes removed*

$$\eta_r(x,y,t) = \eta_d - \sum_q \eta_q \tag{13}$$

The temporal correlation $r(\eta_q, \eta_r)$ *assesses whether the mode SLA is accurately representing the amplitude of the waves. If (1) the SLA signal actually associated with a given mode* q *is well represented by the mode SLA, and (2) other signals are not significantly correlated with variations due to mode* q*, then* $r(\eta_q, \eta_r)$ *should be insignificant especially at latitudes where the wave amplitude peaks. It is important to note that condition (2) may not be met, as other signals that were not projected in this method may have SLA variations that are correlated with the projected modes (e.g., higher-order meridional and baroclinic wave modes, MJO-related variations that do not project onto an equatorial wave mode but are coincident with mode forcing). However, it is expected that for the*

most part SLA signals near the equator will be explained either by the long (zonal) wavelength equatorial waves accounted for in this analysis, or shorter wavelength signals that are uncorrelated with equatorial long wave activity.

These correlation analyses were used to tune the variable parameters w and $\mathbf{\Lambda}$. The correlation values for the optimal parameters given in Section 2.3 are mapped for the equatorial Indian Ocean in Figures 2 and 3. For the Kelvin wave mode ($q = -1$), the correlation $r(\eta_q, \eta_d)$ is highest along the equator (Fig. 2a), while for the Rossby wave mode $q = 1$ the correlation is highest near the latitude of the wave's peaks, 3°–4° north and south of the equator (Fig. 2b). The SLA fields were also bandpassed for intraseasonal frequencies (20–150 day periods) to focus on freely-propagating waves that are forced by and interact with MJO winds (e.g., Han et al., 2001). Compared to lower-frequency equatorial waves, it is easier to resolve the zonal wavenumbers of intraseasonal equatorial waves, and therefore their propagation characteristics. The correlations at these frequencies (Fig. 2c,d) are slightly lower in magnitude than for the non-bandpassed mode SLA, but still peak at the expected latitudes, confirming that c = 2.5 m s^{-1} is a suitable choice for defining the meridional structure of these lowest-mode waves. Moreover, the non-bandpassed $q = 1$ correlations have some maxima slightly equatorward of their expected latitudes (Fig. 2b), but the bandpassed correlation maxima track the expected latitudes for c = 2.5 m s^{-1} nearly exactly (Fig. 2d). The 2.5 m s^{-1} phase speed is consistent with the Argo-based 1st baroclinic mode phase speed estimate by Nagura and McPhaden (2012); according to the estimate by Drushka et al. (2010), also based on Argo data, this value would lie between the 1st and 2nd baroclinic mode Kelvin wave phase speeds (2.8 and 1.8 m s^{-1} respectively). As Drushka et al. (2010) and others have found, the first and second baroclinic modes make substantial contributions to intraseasonal wave activity in the equatorial Indian Ocean, so the 2.5 m s^{-1} phase speed value may represent waves that contain both baroclinic modes.

The Kelvin and $q = 1$ Rossby mode SLA correlations with the residual SLA (Figure 3) suggest that a consideration of timescales is important when tuning the parameters w and $\mathbf{\Lambda}$ to optimize the accuracy of the mode SLA. The non-bandpassed Kelvin wave mode SLA correlation in particular (Fig. 3a) indicate banded features in the northwest Indian Ocean that have little to do with the Kelvin wave structure; it turns out that these are mostly a result of the annual and semiannual signals associated with monsoonal wind reversals. By focusing on correlations with intraseasonal mode SLA (Fig. 3c,d) it is possible to obtain mode SLA values that are not significantly correlated (or only weakly correlated) with the residual SLA near the peak amplitude axes of the waves. The intraseasonal Kelvin wave SLA is slightly positively correlated with the residual SLA along most of the equator, and negatively correlated just off the equator (Fig. 3c); on balance this suggests that there is little bias in the mode SLA estimations of the waves' amplitude. Weak positive or insignificant correlations are also found along the $q = 1$ Rossby wave peak amplitude axes, with negative SLA correlations elsewhere. The exception is north of the equator and west of the longitudes of India/Sri Lanka, where correlations are almost uniformly negative. The negative correlations would imply

that the amplitude of the $q = 1$ Rossby waves are being overestimated in this region, though these inaccuracies in the mode SLA might be explained by interference from the landmasses of Sri Lanka and India.

4 Mode SLA representations of the equatorial ocean

The mode SLA produced by this method has several desirable features compared to earlier techniques used to describe equatorial wave activity. These features include zonal wave propagation that is constrained (though weakly) to within phase speed ranges predicted by theory, and a more active intraseasonal wave field than BM9599 that still has sufficiently long wavelengths ($> 10^\circ$ longitude) to fall within the essentially non-dispersive range of long equatorial wave propagation (e.g. Matsuno, 1966). Figure 4 shows a snapshot of the progression of Kelvin and mode 1 Rossby waves across the Indian Ocean, as tracked by mode SLA during the active El Niño and positive IOD year 1997. During May-July 1997, the period portrayed in Fig. 4, westerly winds along the equator transitioned to anomalously strong easterly winds, forcing an upwelling Kelvin wave along the equator as indicated by negative values of mode SLA (Fig. 4g,h). The reflection of a downwelling Kelvin wave at the eastern boundary (Fig. 4e) is seen as a mode 1 Rossby wave that propagates westward from the boundary to the center of the Indian Ocean (Fig. 4j-l). Furthermore, the propagation characteristics of these waves can be much more readily observed in the mode SLA compared to the raw SLA data.

Hovmöller diagrams of mode SLA amplitudes during 1993–1997 in the equatorial Indian (Figure 5) and Pacific (Figure 6) oceans illustrate wave variations at intraseasonal, annual, and interannual timescales. In the Indian Ocean, Kelvin wave activity largely reflects the annual cycle forced by wind reversals between the northeast and southwest phases of the South Asian monsoon (Fig. 5a); these waves are then generally reflected at the eastern boundary as $q = 1$ Rossby waves (Fig. 5b). The Pacific Ocean Hovmöller diagrams indicate a large amount of interannual as well as intraseasonal wave activity; the dominant signals during the 1997 El Niño (and during the weaker 1994 El Niño before it) are the downwelling Kelvin waves generated, then reflected as downwelling $q = 1$ Rossby waves (Fig. 6a,b). Notably, in the $q = 3$ mode, the Indian and Pacific Ocean basins have overwhelmingly downwelling and upwelling waves respectively during the 1997 El Niño and positive IOD event (Fig. 5d, 6d). This anomaly is not shown consistently in the $q = 1$ modes for each basin (Fig. 5b, 6b), suggesting that the third meridional Rossby wave mode may be as important as the first mode in determining the evolution of the extreme 1997 event.

The amplitudes of the Pacific mode SLA for Kelvin and $q = 1$ Rossby waves are also plotted to illustrate the reflection of equatorial waves at the boundaries (Figure 7). This figure takes the same form and spans a similar time range to Figure 6 in Boulanger and Menkes (1999). In comparing Fig. 7 with the Boulanger and Menkes (1999) figure, it can be seen that the method used here highlights

the higher-frequency intraseasonal wave activity more clearly, such as the downwelling Kelvin waves at the end of 1996 and in early 1997 that initiated the El Niño state. By contrast, the Boulanger and Menkes (1999) wave coefficients contain some non-propagating structure not present in our Figure 7, such as the difference in sign between the western and eastern Pacific (for both Kelvin and Rossby wave coefficients) at the height of the 1997 El Niño. It makes sense that incorporating the zonal propagation of equatorial waves into an SLA projection method would be clearest at intraseasonal frequencies. At annual and longer timescales, Kelvin and lowest-mode equatorial Rossby waves mostly exist as standing features with meridional structures, as the first baroclinic mode of these waves may be in phase across most or all of the basin. But at intraseasonal timescales, the zonal phase propagation is an essential characteristic that may aid in the separation of meridional (and potentially baroclinic) modes of wave activity.

5 Conclusions

The harmonic projection and least-squares method outlined here produces a measure of *equatorial* wave activity that can be *derived* directly *from* satellite observations of SLA. The method *projects onto the data SLA field a set of wave functions that resemble zonally-propagating waveforms, then minimizes a cost function to deconvolve the coefficients of the non-orthogonal wave functions. The result of these calculations is a mode SLA field for equatorial Kelvin waves and the first lowest 5 meridional Rossby wave modes. Correlations of the mode SLA fields with the data SLA and residual SLA fields help to tune the variable parameters in the calculation, and confirm that* $c = 2.5$ *m* s^{-1} *is an accurate choice for the Indian Ocean (1st baroclinic) Kelvin wave phase speed. Compared to the earlier SLA decomposition method used by BM9599 based solely on meridional profiles of the waves, the SLA field generated by this method contains more variability at intraseasonal frequencies, and downplays the role of non-propagating meridional structure in the SLA field. Our method* also allows for some variation in the phase speed of the waves, so a comparison of *the wave amplitudes derived from mode SLA* with the results of linear wind–forced models of equatorial waves (e.g., Yu and McPhaden, 1999; Nagura and McPhaden, 2010) may be useful in studying some weakly nonlinear aspects of Kelvin waves.

One caveat for the use of the mode SLA is that the method favors waveforms that vary at similarly large scales across the ocean basin; near the boundaries or local bathymetric features, it may be desirable to resolve smaller scales more accurately. While the reflection of equatorial waves is quite apparent in our wave amplitude plots (Fig. 5–7), there are cases where an abrupt change in sign occurs from the incoming to the reflected wave. An increase in resolution near the boundaries by incorporating more taper functions in the basis set used could be one way to improve representations of wave reflections. An advantage of the methodological framework described in Section 2 is that like most linear inverse methods it is very adaptable; any signal that has a fairly consistent

structure in one (or two or three) dimensions and propagates in a favored direction could in theory be represented by wave functions of the form given in equation (1). The accurate recovery of the signal using this framework depends on the choice of correct wave function structure and tuning of the cost function against validation metrics.

Acknowledgements. Andrew Delman (ASD) was supported by a NASA Earth and Space Science Fellowship, grant number NNX13AM93H. Janet Sprintall (JS) and Julie McClean (JLM) were supported by NASA award number NNX13AO38G. Lynne Talley (LDT), JLM, and ASD were also supported by NSF grant OCE–0927650. The altimeter products were produced by Ssalto/Duacs and distributed by Aviso, with support from CNES (http://www.aviso.oceanobs.com/duacs/). Computations were carried out on the Geyser cluster within the Yellowstone computing environment hosted by the National Center for Atmospheric Research (NCAR). *We would also like to thank two reviewers for their comments which have helped in improving this manuscript.*

References

Boulanger, J.-P. and Menkes, C.: Propagation and reflection of long equatorial waves in the Pacific Ocean during the 1992–1993 El Niño, J. Geophys. Res., 100, 25,041–25,059, 1995.

Boulanger, J.-P. and Menkes, C.: Long equatorial wave reflection in the Pacific Ocean from TOPEX/POSEIDON data during the 1992–1998 period, Clim. Dyn., 15, 205–225, 1999.

Cane, M. and Sarachik, E.: The response of a linear baroclinic equatorial ocean to periodic forcing, J. Mar. Res., 39, 651–693, 1981.

Delcroix, T., Boulanger, J.-P., Masia, F., and Menkes, C.: Geosat–derived sea level and surface current anomalies in the equatorial Pacific during the 1986–1989 El Niño and La Niña, J. Geophys. Res., 99, 25,093–25,107, 1994.

Drushka, K., Sprintall, J., Gille, S. T., and Brodjonegoro, I.: Vertical structure of Kelvin waves in the Indonesian Throughflow exit passages, J. Phys. Oceanogr., 40, 1965–1987, 2010.

Ducet, N., Traon, P. Y. L., and Reverdin, G.: Global high–resolution mapping of ocean circulation from TOPEX/Poseidon and ERS–1 and –2, J. Geophys. Res., 105, 19,477–19,498, 2000.

Fu, L.-L., Fukumori, I., and Miller, R. N.: Fitting dynamic models to the Geosat sea level observations in the tropical Pacific ocean. Part II: a linear, wind–driven model, J. Phys. Oceanogr., 23, 2162–2181, 1993.

Giese, B. S. and Harrison, D. E.: Aspects of the Kelvin wave response to episodic wind forcing, J. Geophys. Res., 95, 7289–7312, 1990.

Gill, A. E. and Clarke, A. J.: Wind–induced upwelling, coastal currents, and sea–level changes, Deep-Sea Res., 21, 325–345, 1974.

Han, W., Lawrence, D. M., and Webster, P. J.: Dynamical response of equatorial Indian Ocean to intraseasonal winds: zonal flow, Geophys. Res. Lett., 28, 4215–4218, 2001.

Hendon, H. H., Liebmann, B., and Glick, J. D.: Oceanic Kelvin waves and the Madden–Julian oscillation, J. Atmos. Sci., 55, 88–101, 1998.

Kessler, W. S. and McPhaden, M. J.: Oceanic equatorial waves and the 1991–93 El Niño, J. Climate, 8, 1757–1774, 1995.

Long, R. B. and Thacker, W. C.: Data assimilation into a numerical equatorial ocean model. I. The model and the assimilation algorithm, Dyn. Atmos. Oceans, 13, 379–412, 1989a.

Long, R. B. and Thacker, W. C.: Data assimilation into a numerical equatorial ocean model. II. Assimilation experiments, Dyn. Atmos. Oceans, 13, 413–439, 1989b.

Matsuno, T.: Quasi–geostrophic motions in the equatorial area, J. Met. Soc. Japan, 44, 25–43, 1966.

Miller, R. N. and Cane, M. A.: A Kalman filter analysis of sea level height in the tropical Pacific, J. Phys. Oceanogr., 19, 773–790, 1989.

Moore, D. W.: Planetary-gravity waves in an equatorial ocean, Ph.D. thesis, Harvard University.

Nagura, M. and McPhaden, M. J.: Dynamics of zonal current variations associated with the Indian Ocean dipole, J. Geophys. Res., 115, C11026, doi:10.1029/2010JC006423., 2010.

Nagura, M. and McPhaden, M. J.: The dynamics of wind-driven intraseasonal variability in the equatorial Indian Ocean, J. Geophys. Res., 117, C02001, doi:10.1029/2011JC007405., 2012.

Susanto, R. D., Zheng, Q., and Yan, X.-H.: Complex singular value decomposition analysis of equatorial waves in the Pacific observed by TOPEX/Poseidon altimeter, J. Atmos. Oceanic Technol., 15, 764–774, 1998.

Thacker, W. C. and Long, R. B.: Fitting dynamics to data, J. Geophys. Res., 93, 1227–1240, 1988.

Yu, X. and McPhaden, M. J.: Seasonal variability in the equatorial Pacific, J. Phys. Oceanogr., 29, 925–947, 1999.

Yuan, D. and Liu, H.: Long-wave dynamics of sea level variations during Indian Ocean Dipole events, J. Phys. Oceanogr., 39, 1115–1132, 2009.

Yuan, D., Rienecker, M. M., and Schopf, P. S.: Long-wave dynamics of the interannual variability in a numerical hindcast of the equatorial Pacific Ocean circulation during the 1990s, J. Geophys. Res., 109, C05019, 2004.

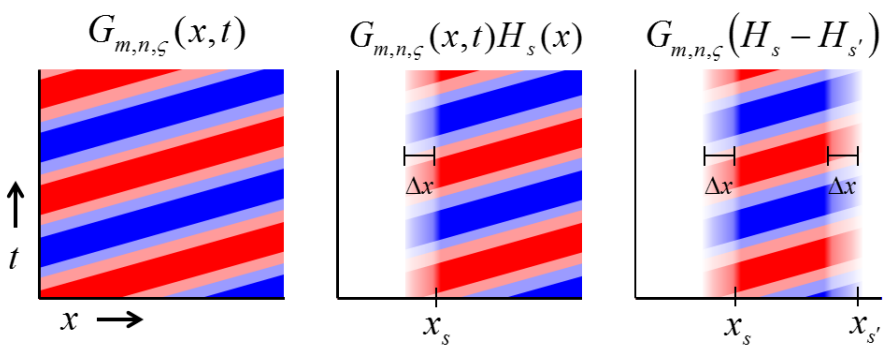

Figure 1. Schematic illustrating the use of taper functions. (a) Profile of a non–tapered harmonic function $G_{m,n,\varsigma}$ in x and t. (b) Profile of the same harmonic function modified or "forced" by a taper function, $G_{m,n,\varsigma}H_s$, with tapering location $x = x_s$ and a tapering window of Δx. (c) Profile of a harmonic function that is "forced" and "dissipated" by two taper functions $G_{m,n,\varsigma}(H_s - H_{s'})$, with tapering locations of $x = x_s$ and $x = x_{s'}$ respectively.

Table 1. Phase speed ranges for zonally-propagating harmonic functions $G^q_{m,n,\varsigma}$ associated with mode q. Positive (negative) values indicate eastward (westward) propagating harmonic functions. For each mode, c_{min} and c_{max} are the minimum- and maximum-magnitude speeds in the range, regardless of direction, i.e., $c_{\text{min}} \leq f_n/k_m \leq c_{\text{max}}$ for Kelvin waves ($q = -1$) and $c_{\text{max}} \leq f_n/k_m \leq c_{\text{min}}$ for Rossby waves ($q > 0$).

Mode q	c_{min}	Theoretical phase speed	c_{max}
-1	+0.6c	+c	+1.4c
1	-c/4	-c/3	-c/2
2	-c/6	-c/5	-c/4
3	-c/8	-c/7	-c/6
4	-c/10	-c/9	-c/8
5	-c/12	-c/11	-c/10

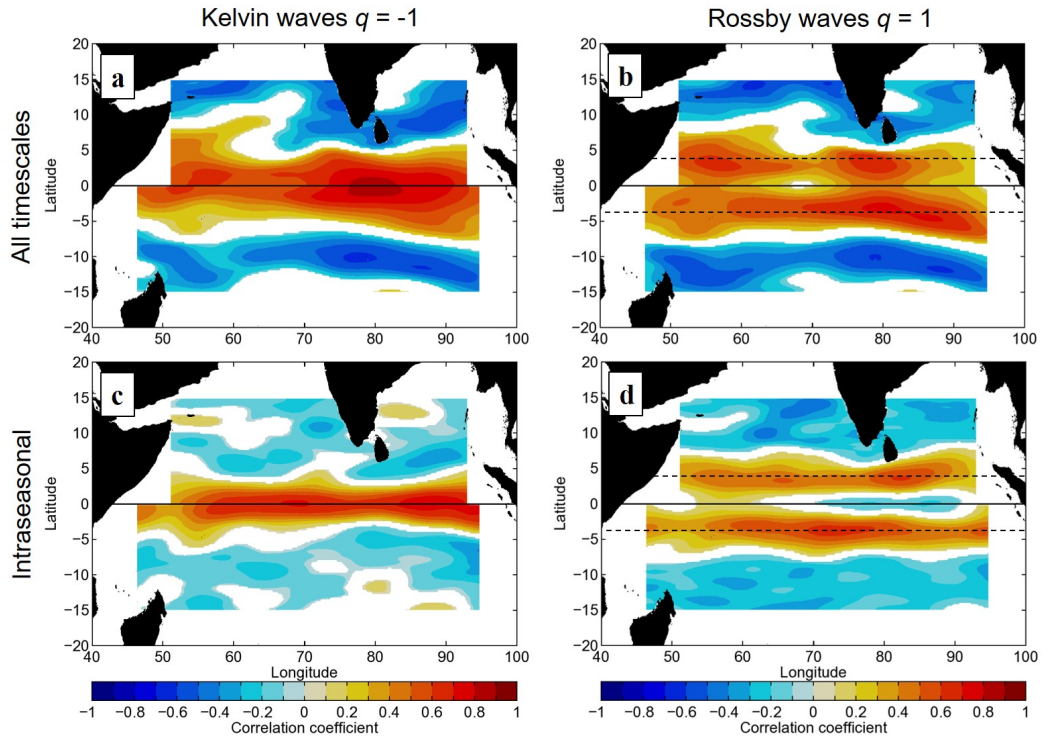

Figure 2. (a) Temporal correlation $r(\eta_q, \eta_d)$ of the Kelvin wave mode SLA ($q = -1$) with the meridionally detrended SLA from the AVISO 1/4° daily gridded product, for the time range 1993–2015. A zonal low-pass filter is applied to η_d prior to computing the correlations, to remove wavelengths shorter than 10°. Only correlation coefficients surpassing the 95% confidence threshold for significance are shaded. (b) Same as (a), but for the correlation of the first meridional mode Rossby wave SLA ($q = 1$) with the meridionally detrended AVISO data. The horizontal dashed line indicates the latitude at which the peak amplitudes of the $q = 1$ Rossby wave occur. (c)-(d) Same as (a)-(b) respectively, but the correlations are computed after bandpassing η_q and η_d for intraseasonal frequencies in the 20–150 day period range.

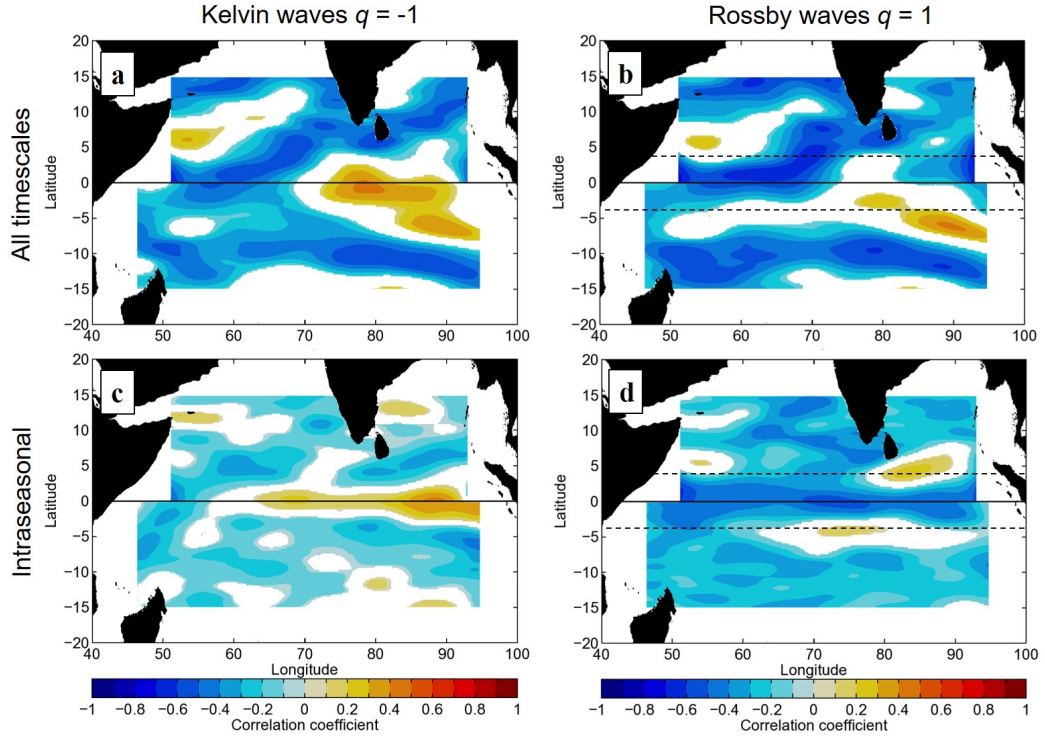

Figure 3. (a) Temporal correlation $r(\eta_q, \eta_r)$ of the Kelvin wave mode SLA ($q = -1$) with the residual SLA unexplained by the Kelvin and Rossby wave mode SLA, for the time range 1993–2015. A zonal low-pass filter is applied to η_r prior to computing the correlations, to remove wavelengths shorter than 10°. Only correlation coefficients surpassing the 95% confidence threshold for significance are shaded. (b) Same as (a), but for the correlation of the first meridional mode Rossby wave SLA ($q = 1$) with the residual SLA. The horizontal dashed line indicates the latitude at which the peak amplitudes of the $q = 1$ Rossby wave occur. (c)-(d) Same as (a)-(b) respectively, but the correlations are computed after bandpassing η_q and η_r for intraseasonal frequencies in the 20–150 day period range.

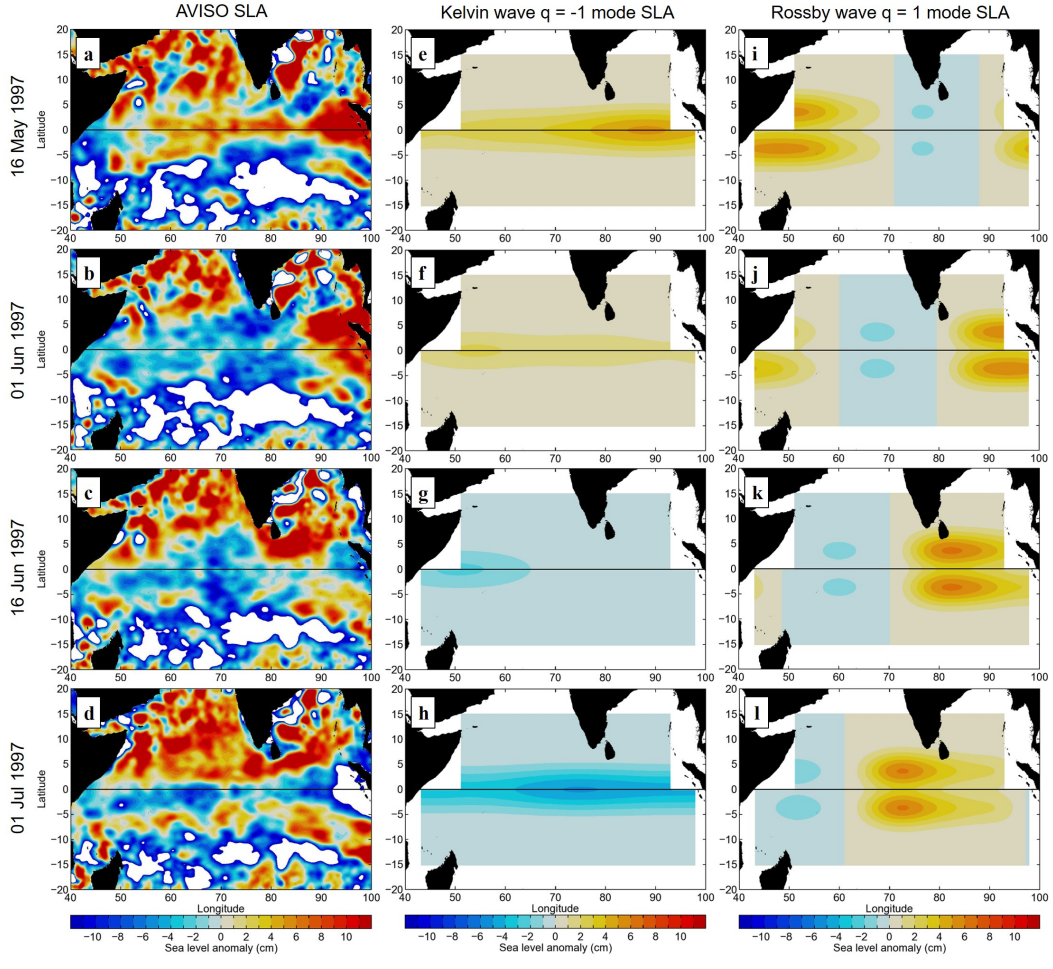

Figure 4. (a)-(d) Maps of the sea level anomaly in the Indian Ocean from AVISO, for a series of dates in May-July 1997. (e)-(h) Maps of the Kelvin wave mode SLA (η_q with $q = -1$) for the same dates. (i)-(l) Maps of the first meridional Rossby wave mode SLA (η_q with $q = 1$) for the same dates.

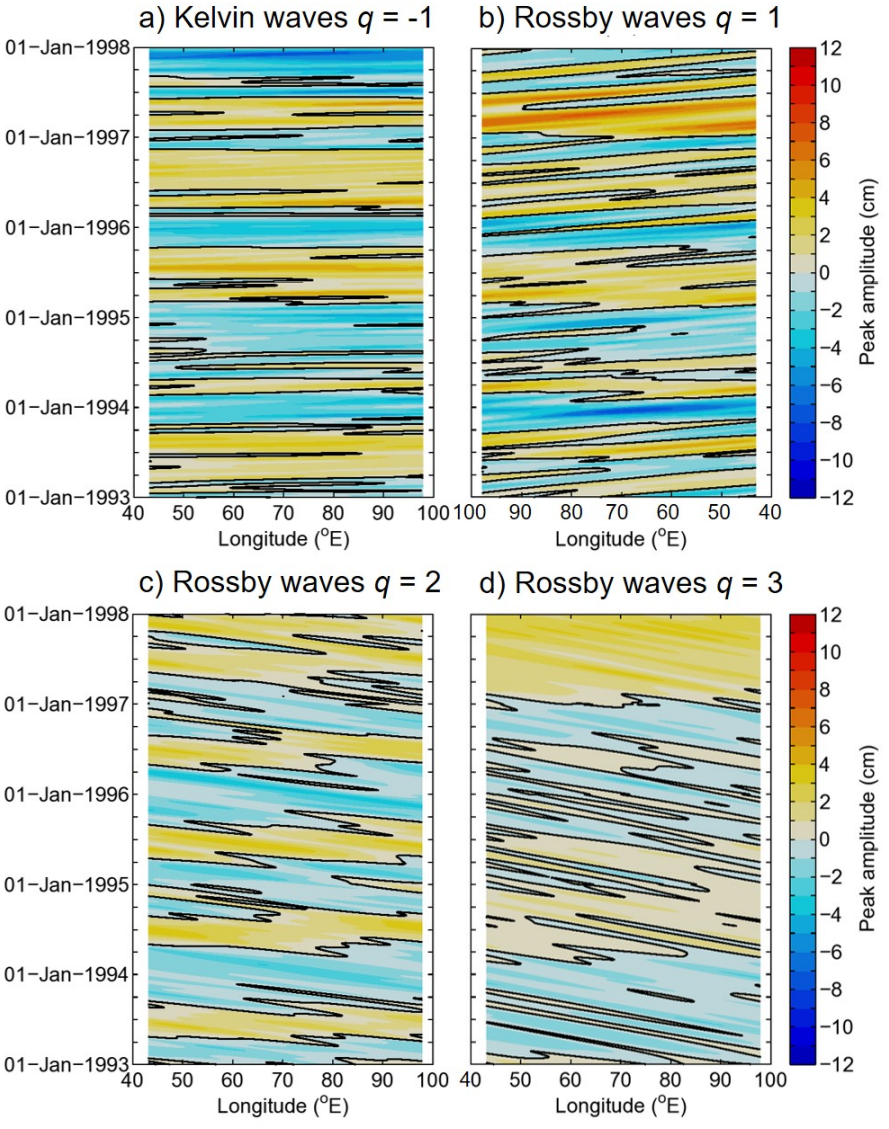

Figure 5. (a) Kelvin wave $q = -1$ mode SLA peak amplitudes (i.e., the mode SLA along the latitude where the wave signal peaks) in the Indian Ocean, plotted from 1993 to 1997. (b) Rossby wave $q = 1$ mode SLA peak amplitudes; in this plot the x-axis is reversed in direction to highlight wave reflection at the eastern boundary. (c) Rossby wave $q = 2$ mode SLA peak amplitudes. (d) Rossby wave $q = 3$ mode SLA peak amplitudes.

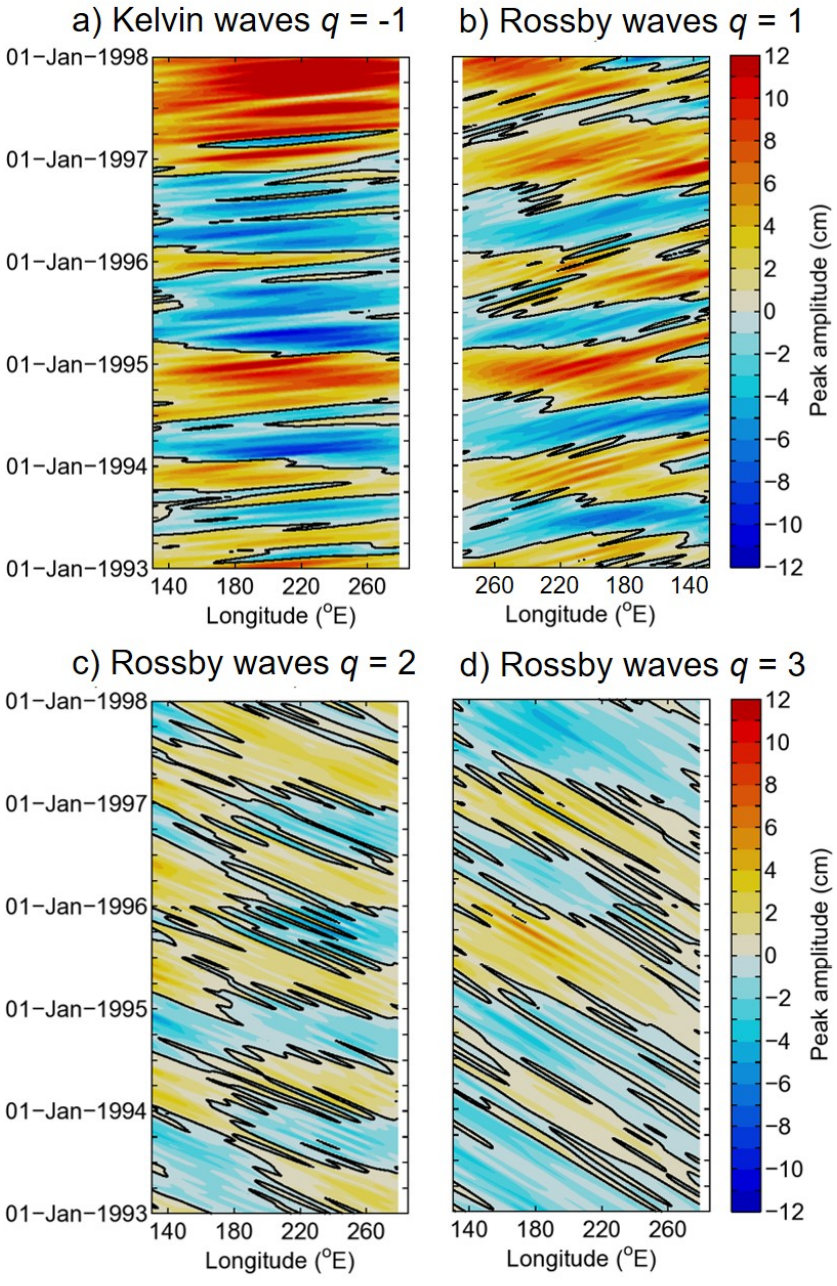

Figure 6. Same as Figure 5, but in the equatorial Pacific Ocean.

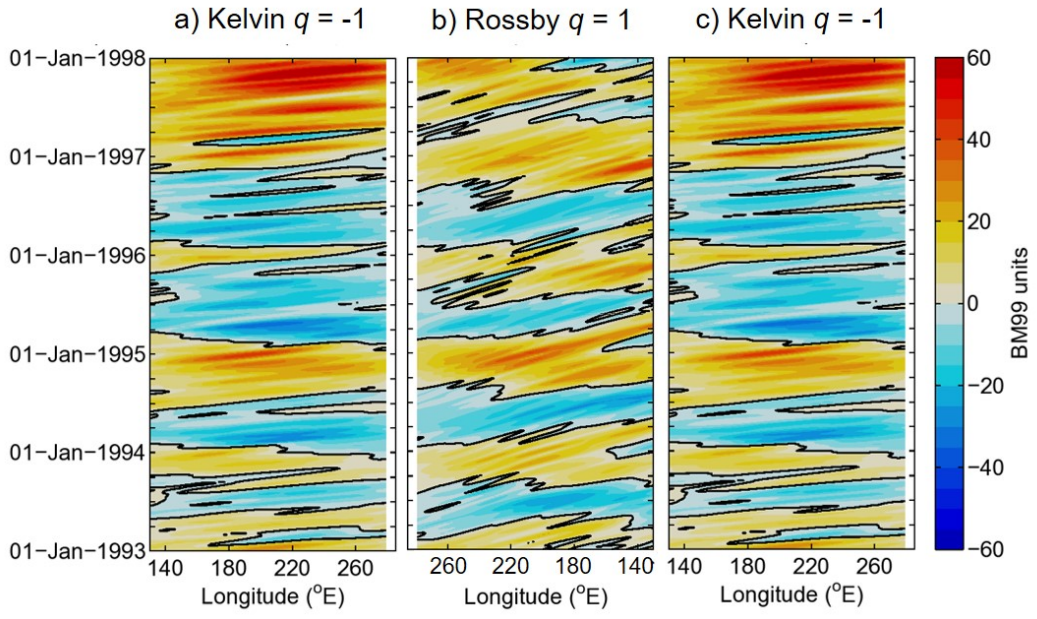

Figure 7. (a) Kelvin wave $q = -1$ mode SLA amplitudes in the equatorial Pacific Ocean, plotted from 1993 to 1997 and normalized in the same way as in Boulanger and Menkes (1999) (1 BM99 unit = 0.32 cm wave amplitude). (b) Rossby wave $q = 1$ mode SLA amplitudes with the x-axis direction reversed; 1 BM99 unit = 0.28 cm wave amplitude. (c) Same as (a). The layout of (a)-(c) highlights the reflection of waves at the eastern and western boundaries; compare to Fig. 6 in Boulanger and Menkes (1999).